ELSEVIER

Test of spike-sorting algorithms on the basis of simulated network data

Kerstin M.L. Menne[a], Andre Folkers[a], Thomas Malina[a], Reinoud Maex[b], Ulrich G. Hofmann[a],*

[a] *Medical University of Lübeck, Institute for Signal Processing, Seelandstr. 1a, D-23569 Lübeck, Germany*
[b] *Born-Bunge Foundation, University of Antwerp, B-2610 Antwerp, Belgium*

Abstract

Results of spike-sorting algorithms are usually compared with recorded signals which themselves underly interpretations, distortions and errors. Our approach is to provide and compare physiological extracellular potential data by a realistic cortical network simulation. For this purpose, we utilize the neural simulator GENESIS and simulate a region of rat hippocampus containing 90 cells. We are able to "record" simulated extracellular potentials from "virtual electrodes" and produce test data closely resembling multisite neuronal recordings. Our realisitic, artificial data are complex and almost natural in appearance; however, current spike detection schemes appear unable to reliably detect all spikes produced. © 2002 Elsevier Science B.V. All rights reserved.

1. Introduction

Progress in microtechnology development by the European VSAMUEL consortium [5] following the track started earlier at the University of Michigan [2], recently achieved multisite recording probes with 32 electrode sites on multiple purpose silicon probes. This opens the door to acquire neuronal signals which may contain spike

---

* Corresponding author.

E-mail addresses: menne@isip.mu-luebeck.de (K.M.L. Menne), folkers@isip.mu-luebeck.de (A. Folkers), malina@isip.mu-luebeck.de (T. Malina), reinoud@bbf.uia.ac.be (R. Maex), hofmann@isip.mu-luebeck.de (U.G. Hofmann).

trains from hundreds of cells [16]. Obviously, the amount of data acquired in a single experiment requires some type of automation to assign spikes to individual cells. This spike sorting is currently done by several more or less standard methods. However, a rigid assessment of their quality is needed.

Until now, results of spike-sorting algorithms have been compared with recorded signals which themselves underly interpretations, distortions, and errors. An alternative is, to run tests on artificial data generated by adding spike snippets to noisy signals [3]. This method has the advantage of control over data, but is paid for with unphysiological data. Our approach is to mimic physiological extracellular potential data in a biologically realistic network simulation. For this purpose, we utilize the freely available neural simulator GENESIS [1] to simulate a small network of 90 cortical cells and use their output for assessment within two automated spike detection algorithms [10,17].

2. Methods

A region of cortex is represented by 72 CA3 pyramidal cells (PYR), randomly spaced at 35 up to 45 µm in each direction, and 18 interspersed inhibitory interneurons. The interneurons are divided into nine feedforward and nine feedback interneurons. The only difference between the two inhibitory cell types is their pattern of connectivity. Neurons of one group are 75–85 µm in x-direction and 155–165 µm in y-direction apart from each other, thus alternating in y-direction. Additionally, there is a random rotation of each cell about its z-axis (see Fig. 2 inset). In the case of the PYR, we employed the Traub model [13] as implemented by Pulin Sampat (Brandeis University) and Patricio Huerta (MIT). This model comprises 66 compartments, thereof one axon initial segment and one axonal compartment. Six different channel types are simulated, namely active Na^+, active Ca^{2+}, delayed rectifier, transient, slow AHP and rapid Ca^{2+}—and voltage-dependent K-channels. We implemented Traub's cortical interneuron model [14] in GENESIS-code by ourselves and incorporated 48 compartments, again including one axon initial segment and one axonal compartment. Channel types, their kinetics and random variation of the resting membrane potential between −65 and −60 mV are the same as in the case of the PYR. The models for PYR and interneurons mainly differ in cell geometry and their channel conductances [14]. Our GENESIS implementation of the two models allows almost exact replication of some results presented in the literature [13,14].

The ratio of 1:4 between interneurons and PYR is orientated to the literature [15], where the ratio is approximately 1:5. We realized the synaptic interactions by spreading the following receptors already implemented in GENESIS: AMPA [4], NMDA [4], $GABA_A$ [8] and $GABA_B$ [12] receptors on the pyramidal cells and AMPA receptors only on the interneurons. The distribution of these receptors allowed the pattern of connectivity shown in Fig. 1.

PYR receive random afferent input at the perisomatic region, feedforward interneurons (FF) at their apical dendrites. FF contact the PYR at the distal, apical and basal dendrites. Excitatory contacts (open triangles) from other PYR are also made in these regions. Soma and proximal dendrites are the targets for the inhibitory input
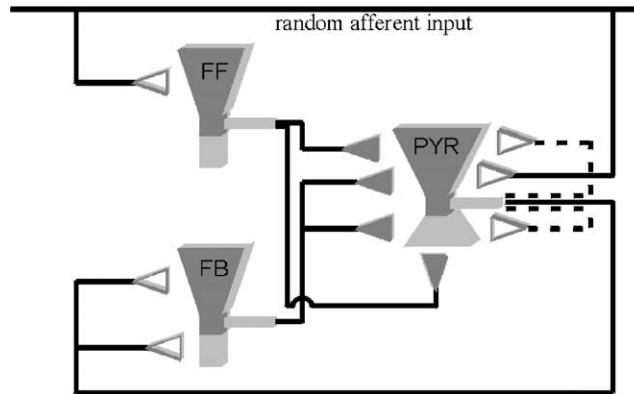
Fig. 1. Sketch of our cortical circuit: (PYR) receive random afferent input at the perisomatic region, feedforward interneurons (FF) at their apical dendrites. FF contact the PYR at the distal apical and basal dendrites. Excitatory contacts (dashed lines with open triangles) from other pyramidal cells are also made in these regions. Soma and proximal dendrites are the targets for the inhibitory input (dark triangles) from FB.

(dark triangles) from feedback interneurons (FB). Cell connections are sparse, but each neuron in the network can contact all other neurons. PYR axons are myelinated, thus getting an assigned conduction velocity of 0.5 m/s. We assigned to unmyelinated interneuron axons and mossy fibers a conduction velocity of 0.2 m/s. Mossy fiber input or afferent input, respectively, is simulated by GENESIS objects randomly generating spikes at a predefined rate. For our simulation, a rate of 40 spikes/s worked out fine. Higher rates led to an excessively high excitation of the network, expressed by continuous oscillations. To prevent this undesired state, we also had to reduce the number of PYR–PYR connections and to increase number and weight of inhibitory connections.

Within the framework of this network simulation, extracellular field potential data can now be generated by simulating multisite electrodes with the help of linearly arranged GENESIS "efield" objects at arbitrary positions in the network. The "efield" object is the implementation of the following Eq. (1) by Nunez [9]

$$F = \frac{1}{4\pi s} \sum_{i=1}^{n} \frac{I_i}{r_i}. \tag{1}$$

The transmembrane currents I_i of n compartments are added with respect to their distance r_i from the "electrode". The scale factor s denotes conductivity. Homogeneous resistivity and no capacitance is assumed for the intercellular medium. A virtual reality (VR)-view of 32 such electrodes, arranged linearly on four needle-like virtual carriers (so called probes) is shown in Fig. 2.

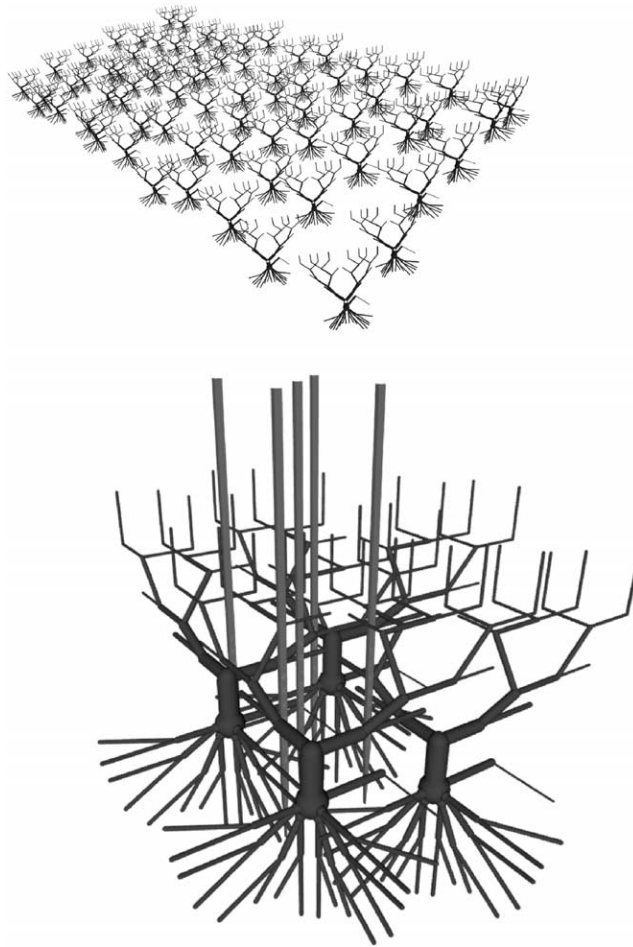The simulation is numerically solved with the exponential Euler integration method and a step size of 2.5 ms.

Fig. 2. VR-view depicting the arrangement of GENESIS efield objects, simulating four probe shafts with eight recording sites each, surrounded by four PYR as part of the geometrical arrangement of the whole cell array. The figures' inset illustrates a VR-view of our array of 72 PYR cells. A random rotation of each cell about its z-axis is not visible in this illustration.

3. Results and discussions

Whereas our small cortical model awaits its physiological validation by real brain recordings, the simulated extracellular, multiunit signals resemble closely experimental multisite recordings taken with silicon probes by [16]. Specifically, a bell-shaped distribution in potential amplitude along a linear site array (Fig. 3) can be found corresponding to real recordings as well. The middle electrode (i.e. GENESIS efield-object No. 4 of each array, see Fig. 2) is located close to simulated cells' soma level and therefore shows the highest amplitude recorded at one time.

Fig. 3. Exemplary recording from seven linearly arranged virtual electrodes of one probe (spacing 30 μm). The horizontal scale bar represents 0.1 s. Note: The maximum amplitude is recorded at roughly the z-coordinate of the closest cells' soma and decays up and down the linear probe array.

In general, the soma is primarily assumed to be the origin of spike activity [6], but is by far the largest compartment as well, both factors may contribute to the high amplitude on the middle trace. Nevertheless, due to an increasing distance to all big, spiking compartments further up and down the linear array, amplitudes recorded there decrease with increasing distance.

However, one discrepancy to the real recordings can be seen in the almost equal amplitude height for all "visible" cells recorded. This discrepancy is most likely due to the fact that the GENESIS efield object does not provide a direction-sensitive parameter, but instead sums over all compartments of the whole surroundings. This is not found with real silicon multisite probes, having their recording sites shielded to the backside by a silicon substrate and thus providing higher sensitivity to one side with yet unknown directional characteristics. Consequently, a comparison of recorded and simulated multisite data may in future shed light on the question of directional characteristics and performance of different recording sites and carriers without the need to sacrifice more than one animal.

A more detailed example of one such multiunit recording trace is shown in Fig. 4 in addition to the four closest PYR and the closest feedback interneuron with its spike train, as indicated by the simulations' output. The combination of displays demonstrates one of our models' drawbacks: a strong tendency for the PYR to fire in groups, yet another reason for ongoing research and an additional obstacle for all automated spike detection schemes. This synchronous firing is obviously not clearly detectable in the
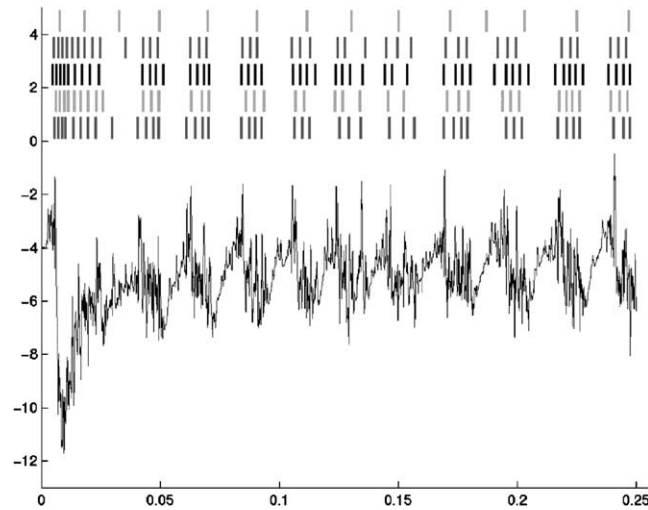
Fig. 4. A recording trace of one site is displayed simultaneously with the spikes of surrounding cells as indicated by the simulator: On top, one FB interneuron (FB4), followed by four different PYR (PYR 39, 38, 33, 32).

multiunit activity, but very clear on spike raster plots. The only multiunit evidence for the synchronous activity can be found in a general rise in background activity, lifting the overall multiunit potential, but seems with all its details not easily back projected to its originating spike trains.

Fig. 4, therefore, clarifies the difficulties faced by whatever type of spike detection. Even though the simulations' output gave precise timing and distribution of spike trains per neuron, those spikes are by far not easily detected in the multiunit activity recorded. But this difficulty is even dwarfed by the necessary second stage to be achieved by each type of automated analysis: the assignment of detected spikes to unique sources, thus producing cellular spike trains much like the one our simulation gives naturally.

In order to assess the first stage of the mentioned backward problem (going from potential data to spikes) in a practical way, we had two different spike detection algorithms competing against each other on the same data set (Fig. 3). One is taken from the freely available software "Spiker" [10] and the other is our own algorithm, based on morphological filters [17].

Fig. 5 displays exemplary spike trains found by Spiker (a) or our detection scheme (b) in relation to the spike trains given by the simulation (c)–(g). In order to mark hits by either of the algorithms, we marked the appropriate spike either on top ("Spiker hit") or on the bottom ("Morph hit"). This way, the better performance of our detection scheme is clearly visible.

Overall results are encouraging, since Spiker recognizes approximately $66 \pm 5\%$ of all spikes, whereas our morphological approach even reaches $80 \pm 4\%$. The better result in the latter case may be explained by the optimization to a dense linear recording array, while Spiker is optimized to a tetrode arrangement, the cross-like arrangement
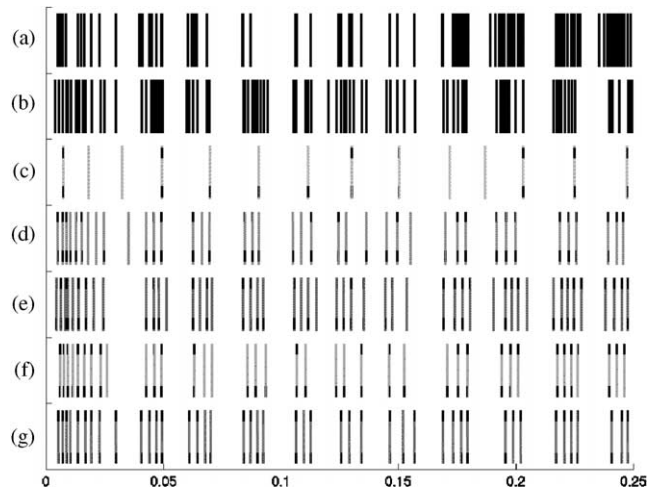
Fig. 5. Spike trains as detected by "Spiker" (a) and our morphological filter tool (b). The following trains represent the "real" simulated spikes and indicate the hits by each detection method: upper black marks indicate a hit by Spiker, lower black marks indicate a hit by our morphological tool. Data from top: FB4 (c), PYR 39 (d), PYR 38 (e), PYR 33 (f), PYR 32 (g).

of sites. No attempts to quantify higher order errors were undertaken at this stage, but are planned for the future.

To summarize the above results, we were able to simulate realistically a small network of cortical cells, thus providing simulated multisite potential data and the means to precisely quantify the performance of spike detection schemes. Future work with this simulation will show whether or not there is a Gold Standard algorithm for automated spike detection and sorting. Incorporating this network model in a finite element [11] description of a brain region [7] may even enable us to finally understand in detail, why real multisite signals look the way they do.

Acknowledgements

References

[1] J.M. Bower, D. Beeman, The Book of GENESIS, 2nd Edition, Springer, New York, 1998.
[2] G. Buzsaki, R. Bickford, et al., Multisite recording of brain field potentials and unit-activity in freely moving rats, J. Neurosci. Meth. 28 (3) (1989) 209–217.
[3] R. Chandra, L. Optican, Detection, classification, and superposition resolution of action potentials in multiunit single-channel recordings by an on-line real-time neural network, IEEE Trans. Biomed. Eng. 44 (5) (1997) 403–412.
[4] F. Gabbiani, J. Midtgaard, et al., Synaptic integration in a model of cerebellar granule cells, J. Neurophysiol. 72 (2) (1994) 999–1009.

 [5] U.G. Hofmann, E. De Schutter, et al., On the Design of Multi-site Microelectrodes for Neuronal Recordings. in MICRO.tec 2000. VDE Verlag, Hannover, FRG, 2000.
 [6] E.R. Kandel, J.H. Schwartz, et al., Principles of Neural Science, 3rd Edition, Prentice-Hall, London, 1991.
 [7] B.H. McCormick, W. Koh, et al., Geometric modeling of local cortical networks, Neurocomputing 32–33 (2000) 461–469.
 [8] R. Miles, Variation in strength of inhibitory synapses in the CA3 region of guinea-pig hippocampus in vitro, J. Physiol. (London) 431 (1990) 659–676.
 [9] P.L. Nunez, Electric Fields of the Brain: The Neurophysics of EEG, 1st Edition, Oxford University Press, Oxford, 1981.
[10] S. Rebrik, B.D. Wright, et al., Spiker–a free GUI program for tetrode spike clustering, http://mccoy.ucsf.edu/Software/Spiker/spiker.html, 2001.
[11] J.N. Reddy, An Introduction to the Finite Element Method, McGraw-Hill, New York, 1984.
[12] H. Suarez, C. Koch, et al., Modeling direction selectivity of simple cells in striate visual cortex within the framework of the canonical microcircuit, J. Neurosci. 15 (10) (1995) 6700–6719.
[13] R.D. Traub, J.R. Jefferys, A branching dendritic model of a rodent CA3 pyramidal neurone, J. Physiol. 481 (1) (1994) 79–95.
[14] R.D. Traub, R. Miles, Pyramidal cell-to-inhibitory cell spike transduction explicable by active dendritic conductances in inhibitory cell, J. Comput. Neurosci. 2 (1995) 291–298.
[15] R.D. Traub, S.B. Colling, et al., Cellular mechanisms of 4-aminopyridine-induced synchronized after-discharges in the rat hippocampal slice, J. Physiol. 489 (1) (1995) 127–140.
[16] S.D. Van Hooser, U.G. Hofmann, et al., Relationship between field potentials and spike activity in rat S1: multi-site cortical recordings and simulations, Neurocomputing 32–33 (2000) 591–596.
[17] B. Weber, T. Malina, et al., Handling large files of multisite microelectrode recordings for the European VSAMUEL consortium, Neurocomputing 38–40 (1–4) (2001) 1725–1734.